Volume 150
Number 14
21 July 2025
Pages 2957-3226

Analyst

rsc.li/analyst

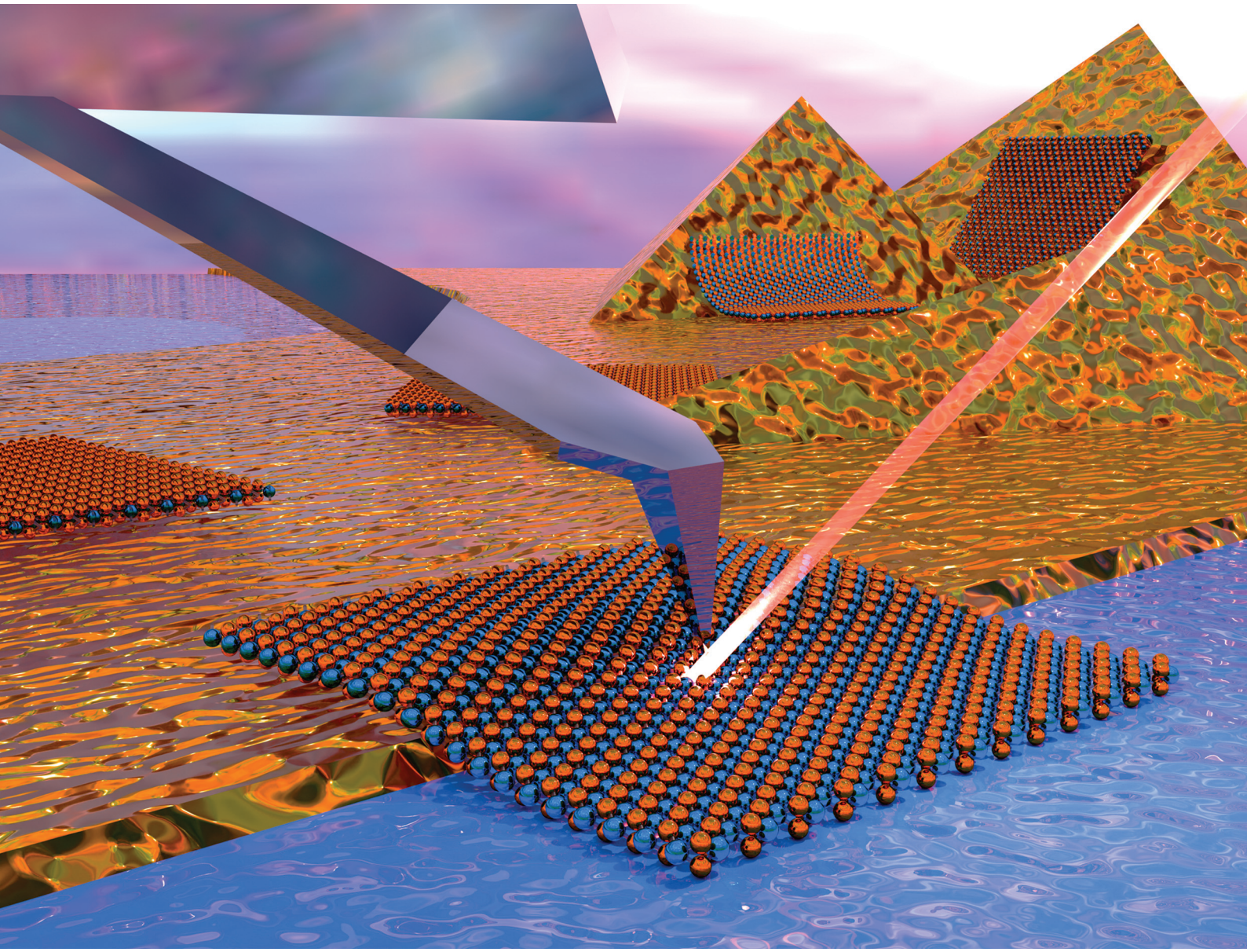

ISSN 0003-2654

ROYAL SOCIETY OF CHEMISTRY

PAPER

James Kerfoot, Graham A. Rance, Michael W. George *et al.* Benchmarking TERS and TEPL probes: towards a reference sample for quantification of near-field enhancement factors in gap and non-gap modes

150 YEARS ANNIVERSARY

Analyst

PAPER

View Article Online
View Journal | View Issue

Cite this: *Analyst*, 2025, **150**, 3077

Benchmarking TERS and TEPL probes: towards a reference sample for quantification of near-field enhancement factors in gap and non-gap modes†

James Kerfoot, *[a] Elizabeth J. Legge, [b] Amy Collins,[c] Jasbinder Chauhan,[c] Kai Rossnagel, [d,e] Peter H. Beton, [c] Christopher J. Mellor,[c] Andrew J. Pollard, [b] Graham A. Rance *[a,f] and Michael W. George *[f]

Benchmarking the near-field signal enhancement attained using plasmonic metal-coated atomic force microscopy (AFM) probes for tip-enhanced Raman spectroscopy (TERS) and tip-enhanced photoluminescence (TEPL) measurements is challenging given the absence of a suitable reference sample that is simple to prepare, easy to use and compatible with different instrument configurations. To this end, in this study, we have fabricated a flake of monolayer tungsten diselenide (1L-WSe_2) stamped across the interface of gold and silver thin films on silicon dioxide and glass. We have demonstrated these samples to be effective for the facile determination of near-field Raman and photoluminescence contrast factors in both gap and non-gap mode, respectively. We show that the near-degenerate E^1_{2g} + A_{1g} and 2LA(M) peaks in the Raman spectra of WSe_2 enable quantification of Raman contrast factors, with a ~1.6-fold increase in TERS signal enhancement in gap mode, relative to non-gap mode, observed for a typical probe. Similar differences in the photoluminescence contrast factors were observed comparing in-contact and out-of-contact signal intensity ratios from gap and non-gap mode TEPL measurements. Moreover, in developing a reference methodology we found that the line shape of the TEPL profile was dependent upon the magnitude of the signal enhancement, with a disproportionate increase in the longer wavelength shoulder of the emission observed in gap mode. As this contribution to the asymmetric line shape is tentatively assigned to a dark exciton, which possesses an out-of-plane transition dipole moment, our TEPL measurements indicate that the directionality of the near-field enhancement provides a further handle enabling quantification of probe performance. Using samples prepared on glass, and comparing results obtained from two different instruments, each with a different excitation laser wavelength and optical access, we demonstrate the universal applicability of our reference material for sensitivity benchmarking of metallised AFM probes in both gap and non-gap mode, suitable for both reflection and transmission geometries, and across the range of laser wavelengths typically used for TERS and TEPL.

Received 24th April 2025,
Accepted 11th June 2025

DOI: 10.1039/d5an00456j

rsc.li/analyst

Introduction

Tip-enhanced Raman spectroscopy (TERS) and tip-enhanced photoluminescence (TEPL) rely upon the electric field enhancement generated at the apex of an atomic force microscopy (AFM) probe coated with a plasmonically-active metal, typically Ag or Au. The field enhancement in the vicinity of the probe apex facilitates the measurement of Raman scattering and/or photoluminescence with nanometre spatial resolution (often <10 nm), which is more than an order of magnitude below the optical diffraction limit, and at near-single-molecule sensitivity.[1–6] As a consequence, over the last two decades, TERS and TEPL have been instrumental in furthering the fundamental understanding of a range of molecular materials at the nanoscale, often providing key insights

[a]*Nanoscale and Microscale Research Centre (nmRC), University of Nottingham, University Park, Nottingham, NG7 2RD, UK. E-mail: james.kerfoot3@nottingham.ac.uk, graham.rance@nottingham.ac.uk*
[b]*National Physical Laboratory (NPL), Hampton Road, Teddington, TW11 0LW, UK*
[c]*School of Physics and Astronomy, University of Nottingham, University Park, Nottingham, NG7 2RD, UK*
[d]*Institut für Experimentelle und Angewandte Physik, Christian-Albrechts-Universität zu Kiel, Olshausenstr. 40, 24098 Kiel, Germany*
[e]*Ruprecht Haensel Laboratory, Deutsches Elektronen-Synchrotron DESY, Notkestr. 85, 22607 Hamburg, Germany*
[f]*School of Chemistry, University of Nottingham, University Park, Nottingham, NG7 2RD, UK. E-mail: michael.george@nottingham.ac.uk*

† Electronic supplementary information (ESI) available. See DOI: https://doi.org/10.1039/d5an00456j

inaccessible by other means, including the identification of active sites in next-generation catalysts,[7,8] the impact of moiré effects on phonon properties in twisted two-dimensional heterostructures,[9] and the distribution of chemical species within biological cells.[10,11]

Despite these advances, TERS and TEPL have not been as widely adopted as might be envisioned. This is, in part, related to difficulties in fabricating probes that routinely deliver the required sensitivity and spatial resolution. In order to try and address this critical issue, there has been extensive research focused on improving the performance of probes for TERS and TEPL through exploration of different preparation methods, including the evaporation of Ag or Au onto AFM probes,[12,13] electrochemical etching,[14,15] attaching Ag nanowires to AFM probes[16,17] and template stripping of Au nanopyramids from etched Si.[18,19] Further improvements in performance have been realised through post-preparation modification of probe morphology and composition, and have included galvanic replacement[17] and controlled oxidation and reduction of probes *via* oxygen plasma/ozone and argon plasma/hydrazine, respectively.[20,21]

Developing and fabricating adequate or improved probes for TERS and TEPL requires appropriate benchmarking of both spatial resolution and signal enhancement. Methods that enable determination of spatial resolution are relatively widespread, relying solely on the measurement of signal response across a feature with small dimensions (often a few nanometres), *i.e.*, an object smaller than the near-field "hotspot" at the probe apex.[5,12,22] For example, one-dimensional nanostructures, such as carbon nanotubes, are widely used to determine the limiting spatial resolution of TERS probes, typically yielding values on the order of ~20 nm,[23] with as low as 1.7 nm reported for carbon nanotubes using ambient STM-TERS.[5] Single molecules have also been spatially discriminated with a resolution of 18 nm using TEPL.[18] However, whilst a comparison of the spatial resolution afforded by a given probe is relatively trivial, the analogous benchmarking of probe sensitivity, *i.e.*, near-field signal enhancement, across reported literature studies is extremely challenging, for a number of reasons. Firstly, the probe sensitivity will critically depend on whether the measurement is performed in gap mode (where the probe is in contact with the material of interest which is on a plasmonic/metallic substrate) or non-gap mode (where the substrate is a dielectric), with gap mode potentially enabling in excess of an order of magnitude higher sensitivity than non-gap mode[24] (Fig. S1 and Table S1, ESI†), though rarely is the same material measured in both modes with the same probe. Secondly, a broad range of materials have been used for the assessment of probe sensitivity, as discussed by Stadler *et al.*,[25] examples include carbon nanotubes,[17] organic dyes,[20] graphene,[19] and self-assembled monolayers (SAMs),[22,26] with the near-field enhancement inevitably displaying material dependence. Thirdly, the signal enhancement is understood to be highly directional[27] resulting in the preferential amplification of modes that are out-of-plane.[28] Finally, there is no single convention adopted by the scientific community to enable quantification and direct comparison of sensitivity. In the majority of cases, when explicitly quoted, benchmarking is accomplished by determining so-called contrast factors (C_R and C_{PL} for Raman and photoluminescence, respectively), defined as C_R or $C_{PL} = (S_{NF+FF}/S_{FF}) - 1$, where S_{NF+FF} and S_{FF} are the signals recorded at the sample surface with either the probe in contact with the surface (*i.e.*, the near-field plus the far-field, NF + FF) or with the probe retracted (*i.e.*, the far-field only, FF), respectively.[12] Alternatively, several studies have reported enhancement factors (EF), defined as C_R multiplied by the ratio of the volumes over which the near-field and far-field spectra are acquired, which may be overestimated due to the approximations made as part of the near-field volume estimation.[29] Together, these factors limit a rigorous comparison of probe sensitivity across literature studies and meaningful conclusions concerning the quantitative performance of the different probe fabrication methods cannot be easily drawn.

Several candidate materials that could, in principle, be used to benchmark TERS and TEPL probe performance have been reported. One such example is, as previously mentioned, carbon nanotubes;[5,12] however, while they are ideal for evaluating spatial resolution in TERS, differences in the near-field Raman signal within and between individual nanotubes due to differing defect densities and resonance effects, respectively, coupled with the absence of a far-field signal in well-dispersed nanotubes, makes accurate quantification of C_R very difficult. More homogeneous samples, such as thin films of poly(3,4-ethylenedioxythiophene) : polystyrene sulfonate (PEDOT : PSS) on glass[12] or SAMs on gold,[8,30] have also been proposed. Whilst C_R of the former can be assessed in both transmission and reflection mode, the latter is typically restricted to reflection mode due to the lack of optical transparency of the substrate, limiting the applicability of such samples to a broad range of setups. A further example is monolayer graphene; however, the in-plane displacements of the most studied D, G and 2D bands do not enable a complete characterisation of C_R for a given probe, which is typically maximal in the out-of-plane direction.[31]

Benchmarking near-field enhancement to allow facile comparison across the research community requires a reference material that is easy to measure, compatible with a range of different experimental set-ups and ideally possesses measurable out-of-plane Raman modes and photoluminescence. In this paper, we present a simple method for the preparation of a monolayer of tungsten diselenide (1L-WSe_2) transferred across the boundary between a Au or Ag layer and a Si or glass substrate, enabling the measurement of C_R and C_{PL} in both gap and non-gap mode. 1L-WSe_2 is a transition metal dichalcogenide (TMD), a class of materials possessing a direct bandgap within the visible range[32] and Raman modes with both in-plane and out-of-plane displacements.[33–35] As such, 1L-WSe_2 represents an ideal candidate material enabling systematic benchmarking of near-field enhancement factors in both Raman scattering and photoluminescence. Our approach has the advantages of (i) requiring no nanoscale alignment to

a particular sample feature *via* AFM, preserving the operational lifetime of the probe, (ii) providing a sample in which material is present within the whole far-field spot, a contribution essential for accurate sensitivity quantification, (iii) allowing quantification of gap and non-gap mode TERS and TEPL within a single sample and (iv) possessing applicability to both reflection and transmission mode geometries across a large window of common excitation laser wavelengths, limited only by the dominance of photoluminescence from 1L-WSe_2 at ~1.65 eV/~750 nm.

Experimental

Sample preparation

Opaque samples for measurement in reflection mode only were fabricated by evaporation of 10 nm of Cr followed by 30 nm of Au, within a thermal evaporator (Moorfield, UK) onto a thermally-grown 300 nm SiO_2/Si substrate (Si-Mat, Germany) through a shadow mask. The thickness of the combined Cr + Au layer was checked using AFM and measured to be 34.2 ± 1.9 nm (Fig. S2, ESI†).

WSe_2 monolayers were prepared by micromechanical cleavage of chemical vapour transport grown bulk crystals onto polydimethylsiloxane (PDMS) (Gel-Pak 3, Gel-Pak, USA) from scotch tape (3M, USA). Large (>10 μm) flakes of 1L-WSe_2 were identified on PDMS based on their contrast under optical microscopy before being aligned to the shadow masked edge of the Au layer on SiO_2 and transferred by viscoelastic stamping[36] using a home-built micromanipulator stage.

Transparent samples for measurement in either transmission or reflection mode were prepared on glass coverslip substrates (0.17 ± 0.01 mm thick, Cole-Parmer, UK) using an analogous approach, by evaporating a 2 nm Ti adhesion layer followed by 10 nm of Au using a shadow mask. The combined thickness of the Au + Ti layers on glass was confirmed using AFM to be 13.1 ± 0.7 nm. A flake of 1L-WSe_2 was then aligned to and transferred on to the glass coverslip and over the edge of the metal layer (Fig. S3, ESI†).

Characterisation with far-field Raman spectroscopy and photoluminescence spectroscopy confirmed the monolayer nature of the 1L-WSe_2 flake in each case (Fig. S4–S6, ESI†).

Probe preparation

Probes were prepared for TERS and TEPL using modifications to the approach detailed by Kumar *et al.*[12] Commercial Si AFM probes (ACCESS-FM, AppNano, USA and HQ:CSC17/No Al, MikroMasch, Bulgaria, for reflection and transmission mode measurements, respectively) were first oxidised to a thickness of ~300 nm by annealing at ~1000 °C for 45 minutes (at National Physical Laboratory, NPL) or 30 minutes (at Nottingham) in water vapour using a tube furnace (Lenton Furnaces, UK at NPL, and Carbolite Gero, UK at Nottingham), then cleaned for 60 minutes using a UV-ozone cleaner (UVOCS®, USA at NPL and Ossilla, UK at Nottingham). Probes for reflection mode measurements (ACCESS-FM) were subsequently metallised *via* electron-beam evaporation (Moorfield, UK) of ~100 nm Ag at a deposition rate of 0.05 nm s^{-1}, a pressure of $<5 \times 10^{-6}$ mbar and an angle of 20° to compensate for the angle of the tip relative to the cantilever. Analogous metallised probes for transmission mode measurements (HQ:CSC17/No Al) were prepared *via* thermal evaporation of ~100 nm Ag at a deposition rate of 0.05 nm s^{-1} and a pressure of 10^{-6} mbar. Additional reflection mode data was also collected using commercially available TERS probes (OMNI-TERS-SNC-Au and OMNI-TERS-FM-Ag, both AppNano, USA).

Measurement setup

Reflection mode TERS and TEPL measurements were performed at the University of Nottingham using a commercial system (LabRAM Nano, HORIBA, France), comprising an AFM (OmegaScope, HORIBA, France) and Raman spectrometer (LabRAM HR Evolution, HORIBA, France) equipped with a 633 nm laser (operated at 142 μW), a 100×/0.7NA metallurgic objective (Mitutoyo, Japan), an edge filter with a low-energy cut off of 50 cm^{-1} and a 150 l mm^{-1} diffraction grating. The lateral drift of the system was measured to be ~0.82 nm min^{-1}. Additional far-field Raman and photoluminescence measurements were performed using a HORIBA LabRAM HR Evolution spectrometer equipped with 532 nm and 633 nm lasers (with maximum powers of 87.9 mW and 15.3 mW, respectively), 100×/0.9NA metallurgic objective (Olympus, Japan) and 150 l mm^{-1}, 600 l mm^{-1} and 1800 l mm^{-1} diffraction gratings. Ultra-low frequency 532 nm measurements (Fig. S4 and S6, ESI†) with a low-energy cut-off of ~10 cm^{-1} were performed using volume Bragg filters.

Transmission mode measurements were performed at NPL using a bespoke system, comprising an AFM (CombiScope, HORIBA, France) and Raman spectrometer (iHR 320, HORIBA, France) equipped with a 532 nm laser (operated at 34 μW and equipped with a liquid crystal radial polarizer), a 100×/1.49NA oil immersion objective (Nikon, Japan) was used in conjunction with type NF immersion oil (Nikon, Japan), a notch filter with a low-energy cut off of ~200 cm^{-1} and a 600 l mm^{-1} diffraction grating.

In both measurement setups, the probe-apex was aligned with the laser beam path and located by scanning the objective lens with the probe in contact with the 1L-WSe_2 flake.

Results and discussion

To enable systematic evaluation of probe sensitivity in both gap and non-gap modes, a flake comprising 1L-WSe_2 (and additional thicker regions) transferred partially over Au and partially over 300 nm SiO_2 on Si was prepared (Fig. 1a–c). The flakes were obtained *via* micromechanical cleaving, thus yielding areas in-excess of (10 × 10) μm^2 on both Au and SiO_2 (Fig. S3, ESI†). Such large flakes, readily visible by optical microscopy (Fig. 1f), enable facile landing of a metallised AFM probe with end-of-tip optical access on the specific region of interest (*i.e.*, 1L-WSe_2 on either Au or SiO_2) without the need

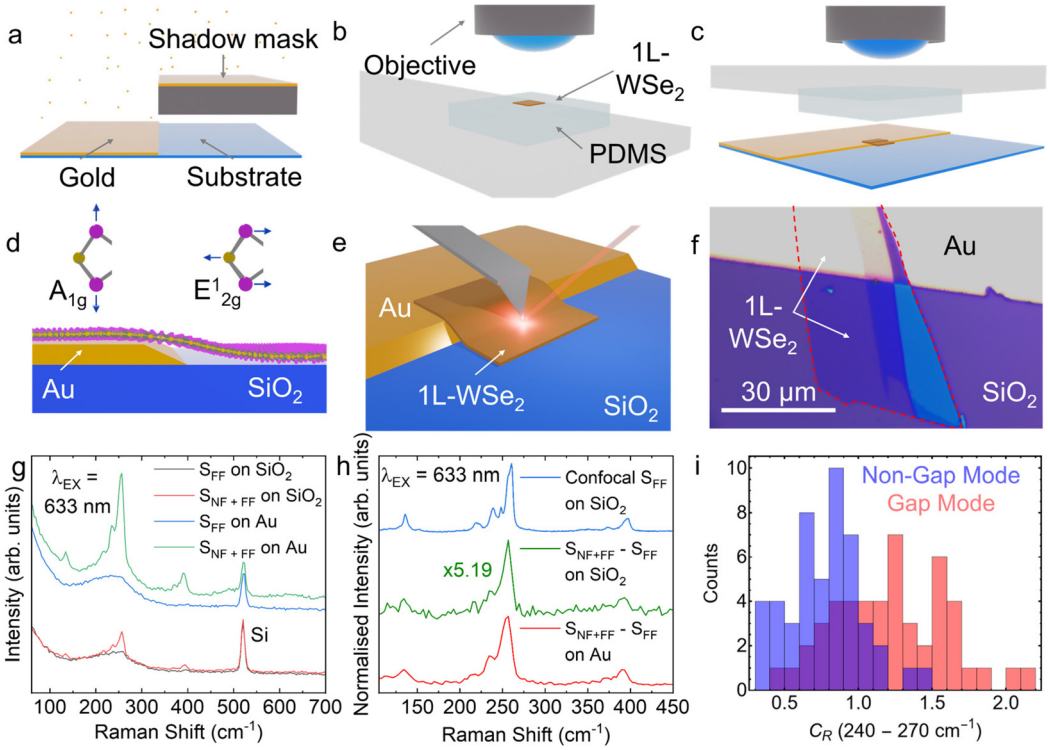

Fig. 1 Schematic representation of the preparation strategy of our reference sample consisting of evaporation of metal onto a substrate through a shadow mask (a), exfoliation of a WSe_2 flake on a viscoelastic PDMS stamp (b) and subsequent transfer onto the interface between the metal and bare substrate using a micromanipulator (c) (Fig. S3, ESI†). This yields an idealised structure (d and e) comprising a 1L-WSe_2 flake overlapping regions of Au and SiO_2 enabling measurement of near-field enhancement in gap and non-gap mode, respectively. Note, these are not drawn to scale and are for illustration purposes only. Insets in (d) are depictions of the symmetries of the degenerate E^1_{2g} (in-plane displacements) and A_{1g} (out-of-plane) Raman modes of WSe_2. Optical microscopy of the sample is shown (f), where the WSe_2 flake has been outlined in red dashes for visualisation, with accompanying far-field spectroscopy measurements (Fig. S4 and S5, ESI†) of the resultant structure permitting identification of monolayer regions of the flake. Single-point spectra acquired with a 633 nm excitation laser with 0.15 mW power, recorded with the Ag probe in contact (S_{NF+FF}) and out-of-contact (S_{FF}) are shown (g). The far-field subtracted TERS spectra (from (g), $S_{NF+FF} - S_{FF}$) were compared relative to a representative far-field spectrum taken at a higher power of 0.77 mW (440% increase in laser power and 50% decrease in acquisition time) on SiO_2 (h). Histograms of C_R (i) extracted from 50 separate measurements of S_{NF+FF} and S_{FF} on areas of SiO_2 and Au show the spread of C_R values obtained in gap and non-gap modes. All contrast ratio values were acquired at lateral distances of >250 nm from the interface between Au and SiO_2.

for an initial AFM reference scan or subsequent TERS mapping – both critically required for common alternative reference samples, such as carbon nanotubes, which are often negatively impacted by drift – thus preserving the lifetime and performance of the probe. Moreover, laser-to-probe alignment can be optimised in direct contact with 1L-WSe_2 using either the TERS or TEPL signal, rather than relying on the inherent, but weak, plasmonic signal from the underlying probe when retracted from the surface, which can be somewhat cumbersome and often requires subsequent re-alignment upon contact of the probe to 1L-WSe_2.

Representative single-point TERS spectra (633 nm excitation laser) acquired from the 1L-WSe_2 regions on Au and on SiO_2 both in- and out-of-contact are shown in Fig. 1g. Both in-contact spectra (S_{NF+FF}) exhibit a clear peak at ~257 cm^{-1}. We tentatively ascribe and later refer to this peak as the 2LA(M) overtone,[33,37] which is typically observed in the literature at ~260 cm^{-1} and known to be enhanced through resonance at 633 nm, though we are careful to note that this peak may be convoluted with additional contributions from resonantly-enhanced second-order processes and phonons at the edges of the Brillouin zone that do not have a common assignation in the literature.[38,39] In addition, a lower wavenumber shoulder was also seen corresponding to the degenerate E^1_{2g} and A_{1g} modes at ~249 cm^{-1} and ~251 cm^{-1}, respectively.[33–35] An assignment of the modes present in higher spectral resolution TERS and confocal Raman spectra with respect to the literature reported values for 1L-WSe_2[33,34,37,40] is shown in Fig. S7 of the ESI.† Our ability to fully deconvolute the complex set of peaks in this region was hindered by the limiting spectral resolution of the 150 l mm^{-1} grating used for TERS measurements (~3 cm^{-1}), which was chosen to enable greater signal for rapid alignment and extraction of the contrast factor. Both the 2LA (M) overtone and the E^1_{2g} and A_{1g} modes are absent in the corresponding far-field spectra in Fig. 1g, obtained under equivalent conditions (S_{FF}), though measurable far-field signal was observed at higher laser powers, which was required for less sensitive (lower C_R) probes in order to deliver a TERS signal

(Fig. S7, ESI†). The peak at ~520 cm^{-1} in all spectra is likely attributed to the SiO_2 substrate along with a possible contribution from the partially exposed Si of the TERS probe. Taking the broad feature in the spectral window of 150–300 cm^{-1} in the far-field spectra (S_{FF} in Fig. 1g) to represent the far-field signal intensity, and to enable more straightforward comparison with data presented later, C_R was extracted *via* Lorentzian fitting of the peak at ~257 cm^{-1} and calculated to be 1.74 ± 0.02 and 0.49 ± 0.01 on Au and SiO_2, respectively, thus yielding a ~3.6-fold increase in the near-field enhancement in gap mode relative to non-gap mode.

To probe the reproducibility of this effect, an area either side of the Au-SiO_2 interface was mapped and C_R was determined from 50 individual measurements on both Au and SiO_2 (Fig. 1i). Differences in the mean C_R obtained from this more statistically appropriate approach were seemingly more modest at 1.2 ± 0.4 and 0.8 ± 0.3 in gap and non-gap mode, respectively, equating to a ~1.6-fold increase in additional enhancement when working in gap mode. We note that, regardless of whether single or multiple point analyses are considered, the enhancement in C_R observed in gap mode relative to non-gap mode is considerably lower than that expected based on consideration of the theoretical differences in electromagnetic field intensities (~10^5 and ~10^9 enhancement relative to far-field Raman signal for non-gap and gap mode, respectively),[41] confirming that additional factors, including chemical effects,[42,43] play an important role in modulating the magnitude of near-field signal enhancement. Moreover, this analysis shows that variation in C_R across multiple measurements on both substrates, whilst not insignificant (31% and 32% standard deviation as a function of the mean C_R for Au and SiO_2, respectively), is effectively independent of the nature of the substrate, *i.e.*, any difference in the local roughness of the Au substrate, relative to SiO_2, does not contribute to additional variability in plasmonic enhancement compared to that seen in non-gap mode. Indeed, the magnitude of variation in C_R observed here is commensurate with that seen in previous interlaboratory studies,[26] with the substrate independence we note likely reflecting a combination of various effects, including a reduction in signal-to-noise (an artefact of the shorter per-point acquisition time necessary when mapping), potential probe degradation inherent when acquiring multiple spectra, nanoscale inhomogeneities in strain and dielectric environment arising from a combination of substrate roughness (seen on both Au and SiO_2) and interfacial contamination above and below the 1L-WSe_2 flake following transfer, as has been seen for related two-dimensional materials in our previous work.[44] In particular, an uneven distribution of polymeric contamination from flake transfer, as discussed in the studies of Jain *et al.*[45] and Rahaman *et al.*,[46] is likely to result in moderate variation in C_R as this will modulate the strength of interactions between Se of 1L-WSe_2 and Au of the substrate[47,48] and/or Ag (or Au) of the probe, all of which in turn will impact the Raman spectrum of 1L-WSe_2.[49] Regardless, we propose the 1L-WSe_2 flake on Au and SiO_2 as a reference sample to quantify C_R in both gap and non-gap modes, obtaining solely single-point measurements in each case. Whilst it is reasonable to expect some variation in C_R when spectra are obtained from multiple locations, single-point measurements permit a facile and accurate assessment of probe performance without impacting the operational lifetime of the probe. Similarly, the evaluation of the inherent Type A uncertainty from the sample itself of ~30% gives prospective users an understanding of the inherent uncertainty that comes with this reference sample when making comparisons between data obtained from the reference sample by the same or different users.

Interestingly, the increase in C_R between SiO_2 and Au observed is contrary to that reported by Miranda *et al.*,[31] who systematically compared C_R of the G and 2D bands of monolayer graphene deposited on glass, Au thin films and Au nanoparticles on different substrates in transmission mode. In their study, negligible differences were observed in C_R for both gap- and non-gap modes across the different substrates explored. This somewhat counterintuitive result was attributed to the electric field in gap mode being preferentially enhanced in the out-of-plane direction and therefore having minimal effect on the in-plane Raman modes of graphene. 1L-WSe_2 possesses both in-plane (E^1_{2g} and 2LA(M)) and out-of-plane (A_{1g}) modes, however, our chosen diffraction grating (150 l mm^{-1} with pixel spacing ~3 cm^{-1}) does not provide sufficient spectral resolution to allow discrimination of the relative intensities of the E^1_{2g}/A_{1g} and 2LA(M) modes. Therefore, commentary on the likelihood of preferential amplification of out-of-plane modes in gap mode is not straightforward; however, this is observed when a higher groove density grating (600 l mm^{-1}) is employed (Fig. S7, ESI†). Such an effect has also been seen in the TERS spectra collected from Au nanostructures as presented by Rahaman *et al.*[46] for 3L-Molybdenum disulfide (MoS_2) and Milekhin *et al.*[50] for 1L-MoS_2. These results indicate that by measuring the relative intensities of in-plane (E^1_{2g} and 2LA(M)) and out-of-plane (A_{1g} and B^1_{2g}) modes of WSe_2, C_R could, in principle, be extracted separately from the in-plane and out-of-plane directions from a single TERS spectrum for any given probe.

In addition to TERS, TEPL spectra were simultaneously recorded from 1L-WSe_2 on Au and on SiO_2. As can be seen in the far-field characterisation of 1L-WSe_2 (Fig. 2a and Fig. S5, ESI†), the emission profile contains a maximum peak at ~1.65 eV/750 nm, which is asymmetric and can be fit using two Lorentzian line shapes (Fig. 2a), centred at ~1.66 eV/746 nm (C1) and at ~1.64 eV/756 nm (C2), which in the far-field spectra predominantly corresponds to signal from neutral excitons and trions, respectively (Fig. 2b). Interestingly, the far-field measurements indicate that the photoluminescence of 1L-WSe_2 on Au was not fully quenched. This is likely due, as discussed previously, to the presence of polymeric contamination at 1L-WSe_2/Au and 1L-WSe_2/air interfaces, an observation typical of the dry transfer process used,[45] and here of significant benefit as it provides another spectroscopic handle to quantify probe performance. As can be seen visually in Fig. 2c, when compared to Fig. 1g, values of C_{PL}, based on single-point measurements, were lower than C_R, with C_{PL} calculated to be 0.5 ± 0.2 and 0.5 ± 0.1 on Au and SiO_2, respect-

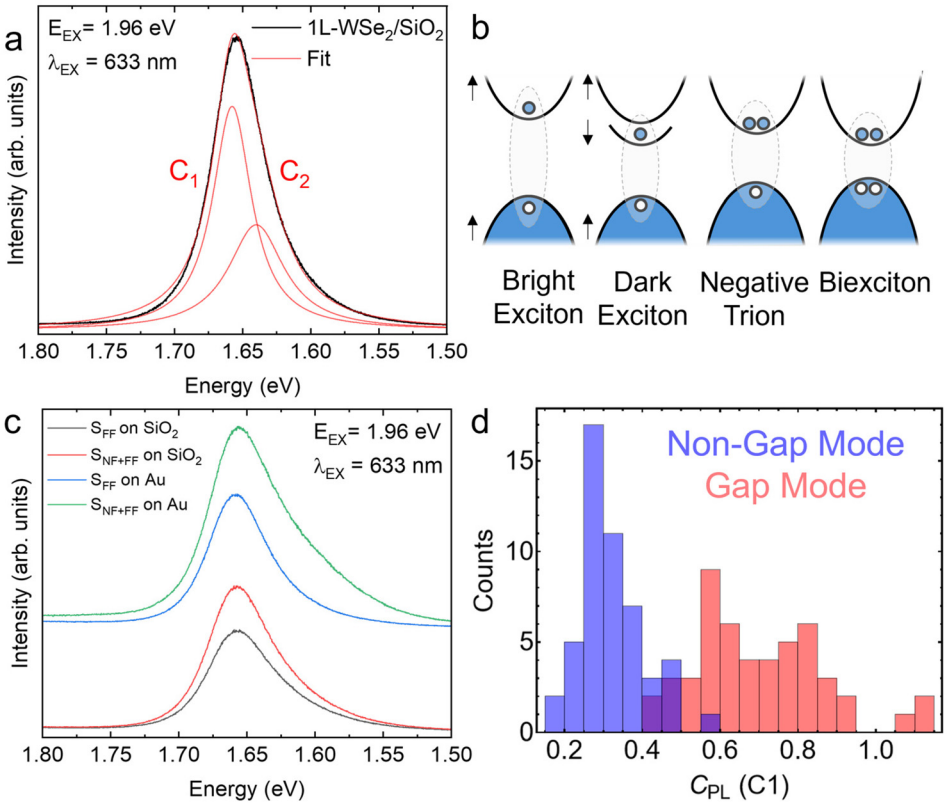

Fig. 2 Single-point photoluminescence spectrum of 1L-WSe_2 on SiO_2 (a) showing contributions from two excitonic species each fit using a Lorentzian line shape along with a simplified band diagram detailing the nature of the excitonic species typically present in monolayer transition metal dichalcogenides (b), where the top and bottom parabolas correspond to the conduction and valence bands of 1L-WSe_2, respectively, blue and white circles correspond to electrons and holes, respectively, arrows denote the alignment of electron/hole spins and dashed ovals denote a bound complex. A comparison of spectra obtained in contact (S_{NF+FF}) and with the probe retracted (S_{FF}) for 1L-WSe_2 on Au and SiO_2 (c), indicates higher C_{PL} in gap mode. Histograms of C_{PL} (d) extracted from 50 separate measurements of S_{NF+FF} and S_{FF} both on SiO_2 and Au show the spread of C_{PL} values obtained in gap and non-gap modes. All measurements were acquired with a 633 nm excitation laser operated at 0.77 mW power for confocal far-field measurements in (a) and 0.15 mW power for TEPL measurements in (c).

ively. Related analysis with an increased number of data points (50) from mapping experiments on both SiO_2 and Au of S_{NF+FF} and S_{FF} (Fig. 2d), generated C_{PL} values of 0.7 ± 0.2 and 0.3 ± 0.1 for Au and SiO_2, respectively, which corresponds to a ~2.3-fold increase in near-field enhancement in gap mode. The variation in C_{PL}, consistent with that seen for the corresponding analysis of C_R as discussed previously, likely reflects a combination of effects encompassing the conditions of the measurement, as well as the fundamental physicochemical characteristics of the probe, sample, and substrate, and their pairwise interactions. It is important to note that in all our measurements the tip was held directly in contact with the surface at each pixel *via* contact mode AFM feedback, such that the mechanical conditions (*i.e.*, tip–sample distance) were consistent between measurements. Whilst it is known that the separation between tip and sample will inevitably lead to variation in measured contrast ratios,[51,52] we do not expect this to be a significant contributor here, but will be important when comparing contact mode AFM with other feedback mechanisms, *e.g.*, scanning tunnelling microscopy.

Interestingly, whilst C_{PL} values are smaller than C_R, more dramatic changes in TEPL line shape are evident. We extract differences in the profile through fitting two Lorentzian line shapes, as seen in Fig. 2a. The higher energy component (C1) is taken to be the neutral exciton while the lower energy component (C2) likely contains contributions from trions, biexcitons and dark excitons, as illustrated in Fig. 2b and discussed later in the main text. We observe a disproportionate increase in the longer wavelength shoulder (C2) of the WSe_2 TEPL across the area defined in the AFM image in Fig. 3a, when in gap mode (Fig. 3b and c). Several effects, including strain,[53,54] doping,[55] dielectric environment,[56] dark excitons[57] and laser power[58] have been shown to affect the far-field line shape of photoluminescence obtained from monolayer TMDs. In addition, more recent reports detail related effects observed in the near-field spectra of analogous materials.[46,59–64] Indeed, in the studies of Park *et al.*,[65] Hasz *et al.*[66] and Rahaman *et al.*,[59] the unique capability provided by AFM to apply force and external bias *via* the probe have been explored. The normalised S_{NF+FF} – S_{FF} and S_{FF} spectra plotted in Fig. 3b each show the average spectrum, from over >256 pixels spanning an area

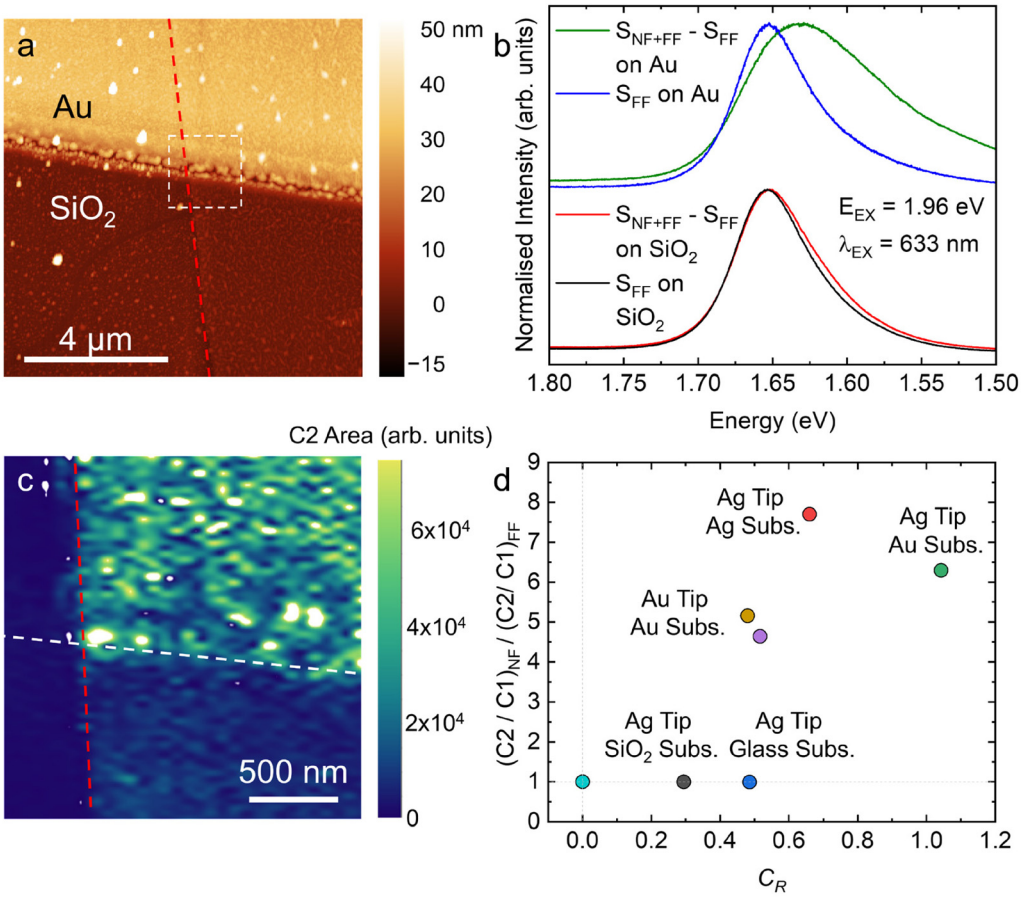

Fig. 3 An AFM image acquired at the intersection of the edge of the 1L-WSe_2 flake and the Au layer (a) is shown in addition to single-point far-field-subtracted TEPL spectra ($S_{NF+FF} - S_{FF}$) and corresponding far-field (S_{FF}) spectra on Au and SiO_2, both of which had been averaged over >256 pixels for each experimental condition (b). A TEPL map (2 μm field-of-view, 31.25 nm pixel size) was acquired from the region illustrated in (a) and a false colour map was generated (c) showing the intensity of the longer wavelength shoulder (C2) extracted by Lorentzian fitting. In both (a) and (c), red lines denote the edge of the 1L-WSe_2 flake. (d) Relative intensities of the possible neutral exciton peak (C1) and the long wavelength shoulder (C2) as a ratio of $S_{NF+FF} - S_{FF}$ compared to S_{FF}, for different probe and substrate materials, are compared to C_R obtained from the same spectra. The normalised $S_{NF+FF} - S_{FF}$ and S_{FF} spectra which were analysed for (d) can be found in Fig. S8 in the ESI.† All measurements were acquired with a 633 nm excitation laser.

comparable to the far-field laser spot size, while the TEPL map (Fig. 3c) shows that the height intensity of the C2 peak (defined in Fig. 2a) is consistently higher on the Au substrate in comparison to that on the SiO_2 substrate, with some additional local variations in the height of the C2 peak observed across the Au and SiO_2 interface. The root-mean square roughness of the 1L-WSe_2 layer on Au (1.6 ± 0.3 nm) and SiO_2 (1.5 ± 0.3 nm) was calculated from an AFM image (Fig. 3a). The similar roughness of the 1L-WSe_2 layer on Au and SiO_2 and the clear differences in the area averaged far-field PL and far-field subtracted TEPL spectra indicate that the difference between the TEPL spectra of 1L-WSe_2 on Au and SiO_2 are a consequence of the near-field enhancement achieved when bringing the plasmonically active probe into contact with the sample, while nanoscale effects, such as surface roughness,[67] local strain,[53,54] dielectric environment[56] and doping variations[55] due to the conformation of the 1L-WSe_2 on the substrate, may account for local variations across uniform Au and SiO_2 regions.

Several explanations have previously been given to account for the emergence of longer wavelength peaks in the TEPL of 1L-WSe_2 and related structures. Tip-induced doping was shown by Su *et al.* to bring about changes in the relative contribution of neutral excitons and negatively charged trions in MoS_2.[62] In both TEPL and systems where TMDs are interfaced on both sides with plasmonic layers, preferential plasmonic enhancement of trion and biexciton species has also been discussed.[60,68–70] More recently, longer wavelength TEPL components have been attributed to spin-triplet dark excitons (Fig. 2b), which are favourably excited in gap mode TEPL owing to their out-of-plane transition dipole moment.[46,60,66,71,72] To gain further insight into the origin of the long wavelength shoulder, TEPL measurements were carried out on 1L-WSe_2 on a range of substrates (Au, Ag, SiO_2

and glass) with both Au and Ag coated probes (Fig. 3d). In all cases, the relative intensity of the low energy shoulder extracted using Lorentzian fitting remained the same or increased in the near-field spectra relative to the corresponding far-field, which is contrary to what one would expect from probe-induced doping given the work functions of Ag, Au and 1L-WSe_2 (~4.3 eV,[73] ~5.1 eV[74] and ~4.5 eV,[55] respectively). To determine the origin of the long wavelength shoulder in our WSe_2 TEPL, *i.e.*, as dark excitons, trions or biexcitons, we investigated the relative intensity (by area) of the different contributions to the TEPL spectra from 1L-WSe_2 on Au across a range of laser powers (Fig. S9, ESI†). The near-linear behaviour of the area of the Lorentzian fitted C1 and C2 peaks as a function of laser power are consistent with a dark exciton for the longer wavelength component, as trions/biexcitons would be expected to show a superlinear/quadratic dependence.[60] Moreover, in Fig. 3d, we plot the increase in the relative intensity of the low energy shoulder in the near-field photoluminescence spectra as a function of the C_R extracted from the same spectra for various combinations of probe material and substrate. This shows that the increase in the relative contribution of the low energy shoulder only occurs in gap mode, which is further evidence that the feature is more likely a dark exciton, which would be preferentially enhanced in gap mode given its transition dipole moment would be aligned to the polarisability of the probe apex/substrate plasmonic nanostructure. These results demonstrate that the existence of power- and polarisation-dependent excitonic processes in 1L-WSe_2 is very useful for benchmarking probe performance, as, in addition to quickly extracting C_{PL} based upon the intensity of the neutral exciton, further information regarding the directionality of the enhancement could be obtained by analysing the line shape of the photoluminescence profile.

Finally, to validate the applicability of the proposed sample configuration to quantify probe sensitivity across different instrument set-ups, *i.e.*, transmission mode as well as reflection mode, TERS measurements were performed using a proposed alternative reference sample on which a 1L-WSe_2 flake was transferred partially over glass and partially over 10 nm of Au (with a 2 nm Ti adhesion layer) on glass (Fig. 4a). The glass substrate and a 10 nm Au layer were chosen to facilitate transmission mode measurements, where the 10 nm Au layer is thinner than the 30 nm Au layer used for reflection mode, as signal will inevitably be attenuated due to absorbance of both the incident and scattered light by Au. The sample was prepared as described in the Experimental section and as shown in Fig. S6 of the ESI.† S_{NF+FF} and S_{FF} spectra were measured from at least three locations in each non-gap mode and gap mode area (five measurements on glass and three on Au were possible within the lifetime of the probe used for testing, and therefore used for analysis) and the spectra corresponding to the median values of C_R are shown in Fig. 4b. We note the intensity of S_{FF} and S_{NF+FF} on Au is lower than that observed on glass due to attenuation of the transmitted laser and Raman scattered signal by Au (a slightly opaque layer within the laser pathway) in this configuration. For both gap mode measurements on Au and non-gap mode measurements on glass, a relative increase in the intensity of the peak arising from the degenerate E^1_{2g} + A_{1g} Raman modes was observed with the TERS probe present, demonstrating that C_R can also be readily extracted from this sample in transmission mode. The mean values of C_R were found to be 0.8 ± 0.4 and 0.5 ± 0.2 for Au and glass, respectively, which is a ~1.6-fold increase in signal due to gap mode enhancement, in good qualitative agreement with our ~1.6-fold increase in signal in reflection mode. Whilst there is more variability in C_R observed in transmission mode (46% and 41% standard deviation as a function of the mean C_R for Au and glass, respectively) compared to reflection mode (31% and 32% standard deviation as a function of the mean C_R for Au and SiO_2, respectively), it is important to note that the number of spectra upon which the transmission mode values are based is significantly smaller than the number in reflection mode. Regardless, the observations made using our modified proposed reference sample in transmission mode are very similar to those obtained in reflection mode and thus clearly demonstrate the versatility of our

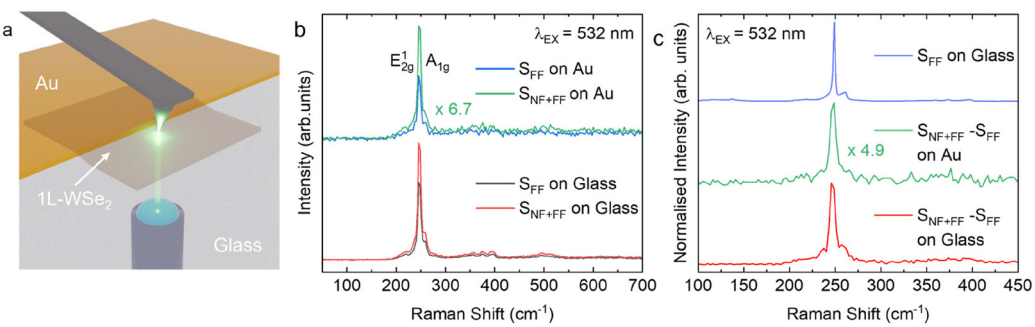

Fig. 4 Schematic representation of a transmission mode TERS measurement of a modified proposed reference sample comprising a 1L-WSe_2 flake overlapping regions of both Au and glass (a). Using probes coated in Ag, spectra acquired with a 532 nm excitation laser were recorded from 1L-WSe_2 on (S_{NF+FF}) and off (S_{FF}) the hotspot of the probe in gap mode and non-gap mode (b). The spectra have been normalised such that the S_{NF+FF} spectra are of equal intensity. For comparison, the normalised far-field-subtracted TERS spectra (S_{NF+FF} − S_{FF}) on Au and glass are shown, along with the far-field Raman signal measured on glass (c). The spectra shown in (b) and (c) are single-point spectra corresponding to the position at which the median enhancement factor was extracted for both Au and glass.

1L-WSe_2-based materials to quantify probe performance irrespective of specific instrument configuration.

Conclusions

We have fabricated and tested a class of proposed reference samples for TERS and TEPL measurements in which a 1L-WSe_2 flake is transferred partially over Au and partially over SiO_2 or glass enabling rapid comparison of the near-field signal enhancement in both gap and non-gap mode all within a single sample. We have seen that the 2LA(M) and combined E^1_{2g} + A_{1g} Raman modes provide an excellent handle for quantification of Raman spectroscopy contrast factors, with a ~1.6-fold amplification in TERS signal enhancement in gap mode, relative to non-gap mode, typically observed. Similar contrast factors are observed using the signal intensities from photoluminescence, with additional analysis showing that the longer wavelength component of the asymmetric TEPL line shape, tentatively ascribed to a dark exciton, is preferentially enhanced in gap mode. The combination of both gap mode and non-gap mode, and the well-defined plane of the 1L-WSe_2 flake, and by extension the Raman mode displacements and photoluminescence transition dipole moments *versus* the probe dipole, enables a greater range of properties to benchmark near-field enhancement than alternative samples, such as disordered polymers and dye molecules. By performing the characterisation using two common access geometries in two separate laboratories, and critically assessing the performance of our reference sample against a guiding set of criteria we consider important for an ideal TERS/TEPL reference sample (Table S2, ESI†), we demonstrate the suitability of this class of sample to be adopted as a future TERS/TEPL reference enabling the refinement of new probe development and benchmarking measurement protocols across different laboratories.

Author contributions

James Kerfoot: conceptualisation, formal analysis, investigation, methodology, writing – original draft, writing – review & editing. Elizabeth J. Legge: formal analysis, investigation, validation, writing – original draft, writing – review & editing. Amy Collins: methodology. Jasbinder Chauhan: methodology. Kai Rossnagel: resources. Peter H. Beton: formal analysis. Christopher J. Mellor: methodology. Andrew J. Pollard: formal analysis, validation, writing – original draft, writing – review & editing. Graham A. Rance: conceptualisation, formal analysis, methodology, funding acquisition, supervision, writing – original draft, writing – review & editing. Michael W. George: methodology, funding acquisition, supervision, writing – original draft, writing – review & editing.

Conflicts of interest

The authors declare no competing financial interests.

Data availability

The data supporting this article have been included as part of the ESI.†

Acknowledgements

JK, GAR and MWG acknowledge funding from the Engineering and Physical Science Research Council (EPSRC) (Project: EP/V053884/1) and support from the Nanoscale and Microscale Research Centre (nmRC). EJL and AJP would like to acknowledge the National Measurement System (NMS) of the Department for Science, Innovation and Technology (DSIT), UK (projects #128826) for funding. The authors thank Dongkuk Kim and Sebastian Wood at the National Physical Laboratory, U.K., for discussion associated with the manuscript.

References

1 R. M. Stöckle, Y. D. Suh, V. Deckert and R. Zenobi, Nanoscale chemical analysis by tip-enhanced Raman spectroscopy, *Chem. Phys. Lett.*, 2000, **318**(1), 131–136, DOI: 10.1016/S0009-2614(99)01451-7.

2 W. Zhang, B. S. Yeo, T. Schmid and R. Zenobi, Single molecule tip-enhanced Raman spectroscopy with silver tips, *J. Phys. Chem. C*, 2007, **111**(4), 1733–1738, DOI: 10.1021/jp064740r.

3 E. Bailo and V. Deckert, Tip-enhanced Raman scattering, *Chem. Soc. Rev.*, 2008, **37**(5), 921–930, DOI: 10.1039/B705967C.

4 E. Bailo and V. Deckert, Tip-enhanced Raman spectroscopy of single RNA strands: towards a novel direct-sequencing method, *Angew. Chem., Int. Ed.*, 2008, **47**(9), 1658–1661, DOI: 10.1002/anie.200704054.

5 C. Chen, N. Hayazawa and S. Kawata, A 1.7 nm resolution chemical analysis of carbon nanotubes by tip-enhanced Raman imaging in the ambient, *Nat. Commun.*, 2014, **5**(1), 3312, DOI: 10.1038/ncomms4312.

6 M. D. Sonntag, J. M. Klingsporn, L. K. Garibay, J. M. Roberts, J. A. Dieringer, T. Seideman, K. A. Scheidt, L. Jensen, G. C. Schatz and R. P. Van Duyne, Single-molecule, tip-enhanced Raman spectroscopy, *J. Phys. Chem. C*, 2012, **116**(1), 478–483, DOI: 10.1021/jp209982h.

7 N. Kumar, C. S. Wondergem, A. J. Wain and B. M. Weckhuysen, In situ nanoscale investigation of catalytic reactions in the liquid phase using zirconia-protected tip-enhanced Raman spectroscopy probes, *J. Phys. Chem. Lett.*, 2019, **10**(8), 1669–1675, DOI: 10.1021/acs.jpclett.8b02496.

8 E. M. van Schrojenstein Lantman, T. Deckert-Gaudig, A. J. G. Mank, V. Deckert and B. M. Weckhuysen, Catalytic processes monitored at the nanoscale with tip-enhanced

Raman spectroscopy, *Nat. Nanotechnol.*, 2012, **7**(9), 583–586, DOI: **10.1038/nnano.2012.131**.

9 A. C. Gadelha, D. A. A. Ohlberg, C. Rabelo, E. G. S. Neto, T. L. Vasconcelos, J. L. Campos, J. S. Lemos, V. Ornelas, D. Miranda, R. Nadas, *et al.*, Localization of lattice dynamics in low-angle twisted bilayer graphene, *Nature*, 2021, **590**(7846), 405–409, DOI: **10.1038/s41586-021-03252-5**.

10 N. Kumar, M. M. Drozdz, H. Jiang, D. M. Santos and D. J. Vaux, Nanoscale mapping of newly-synthesised phospholipid molecules in a biological cell using tip-enhanced Raman spectroscopy, *Chem. Commun.*, 2017, **53**(16), 2451–2454, DOI: **10.1039/C6CC10226C**.

11 D. Mrđenović, Z.-X. Tang, Y. Pandey, W. Su, Y. Zhang, N. Kumar and R. Zenobi, Regioselective tip-enhanced Raman spectroscopy of lipid membranes with sub-nanometer axial resolution, *Nano Lett.*, 2023, **23**(9), 3939–3946, DOI: **10.1021/acs.nanolett.3c00689**.

12 N. Kumar, B. M. Weckhuysen, A. J. Wain and A. J. Pollard, Nanoscale chemical imaging using tip-enhanced Raman spectroscopy, *Nat. Protoc.*, 2019, **14**(4), 1169–1193, DOI: **10.1038/s41596-019-0132-z**.

13 A. Taguchi, J. Yu, P. Verma and S. Kawata, Optical antennas with multiple plasmonic nanoparticles for tip-enhanced Raman microscopy, *Nanoscale*, 2015, **7**(41), 17424–17433, DOI: **10.1039/C5NR05022G**.

14 C. Lee, S. T. Kim, B. G. Jeong, S. J. Yun, Y. J. Song, Y. H. Lee, D. J. Park and M. S. Jeong, Tip-enhanced Raman scattering imaging of two-dimensional tungsten disulfide with optimized tip fabrication process, *Sci. Rep.*, 2017, **7**(1), 40810, DOI: **10.1038/srep40810**.

15 T. L. Vasconcelos, B. S. Archanjo, B. Fragneaud, B. S. Oliveira, J. Riikonen, C. Li, D. S. Ribeiro, C. Rabelo, W. N. Rodrigues, A. Jorio, *et al.*, Tuning localized surface plasmon resonance in scanning near-field optical microscopy probes, *ACS Nano*, 2015, **9**(6), 6297–6304, DOI: **10.1021/acsnano.5b01794**.

16 P. Walke, Y. Fujita, W. Peeters, S. Toyouchi, W. Frederickx, S. De Feyter and H. Uji-i, Silver nanowires for highly reproducible cantilever based AFM-TERS microscopy: towards a universal TERS probe, *Nanoscale*, 2018, **10**(16), 7556–7565, DOI: **10.1039/C8NR02225A**.

17 H. Wen, T. Inose, K. Hirai, T. Akashi, S. Sugioka, J. Li, W. Peeters, E. Fron, B. Fortuni, Y. Nakata, *et al.*, Gold-coated silver nanowires for long lifetime AFM-TERS probes, *Nanoscale*, 2022, **14**(14), 5439–5446, DOI: **10.1039/D1NR07833J**.

18 T. W. Johnson, Z. J. Lapin, R. Beams, N. C. Lindquist, S. G. Rodrigo, L. Novotny and S.-H. Oh, Highly reproducible near-field optical imaging with sub-20 nm resolution based on template-stripped gold pyramids, *ACS Nano*, 2012, **6**(10), 9168–9174, DOI: **10.1021/nn303496g**.

19 T. L. Vasconcelos, B. S. Archanjo, B. S. Oliveira, R. Valaski, R. C. Cordeiro, H. G. Medeiros, C. Rabelo, A. Ribeiro, P. Ercius, C. A. Achete, *et al.*, Plasmon-tunable tip pyramids: monopole nanoantennas for near-field scanning optical microscopy, *Adv. Opt. Mater.*, 2018, **6**(20), 1800528, DOI: **10.1002/adom.201800528**.

20 A. Capaccio, A. Sasso, O. Tarallo and G. Rusciano, Coral-like plasmonic probes for tip-enhanced Raman spectroscopy, *Nanoscale*, 2020, **12**(48), 24376–24384, DOI: **10.1039/D0NR05107A**.

21 V. K. Rao, K. K. H. De Silva and M. Yoshimura, Reversal and control the tip-enhanced Raman scattering efficiency of rough plasmonic probes fabricated using UV-ozone and hydrazine, *Appl. Surf. Sci.*, 2022, **577**, 151937, DOI: **10.1016/j.apsusc.2021.151937**.

22 A. Sacco, D. Imbraguglio, A. M. Giovannozzi, C. Portesi and A. M. Rossi, Development of a candidate reference sample for the characterization of tip-enhanced Raman spectroscopy spatial resolution, *RSC Adv.*, 2018, **8**(49), 27863–27869, DOI: **10.1039/C8RA03762K**.

23 A. Hartschuh, E. J. Sánchez, X. S. Xie and L. Novotny, High-resolution near-field Raman microscopy of single-walled carbon nanotubes, *Phys. Rev. Lett.*, 2003, **90**(9), 095503, DOI: **10.1103/PhysRevLett.90.095503**.

24 J. Stadler, B. Oswald, T. Schmid and R. Zenobi, Characterizing unusual metal substrates for gap-mode tip-enhanced Raman spectroscopy, *J. Raman Spectrosc.*, 2013, **44**(2), 227–233, DOI: **10.1002/jrs.4169**.

25 J. Stadler, T. Schmid and R. Zenobi, Developments in and practical guidelines for tip-enhanced Raman spectroscopy, *Nanoscale*, 2012, **4**(6), 1856–1870, DOI: **10.1039/C1NR11143D**.

26 C. Blum, L. Opilik, J. M. Atkin, K. Braun, S. B. Kämmer, V. Kravtsov, N. Kumar, S. Lemeshko, J.-F. Li, K. Luszcz, *et al.*, Tip-enhanced Raman spectroscopy – an interlaboratory reproducibility and comparison study, *J. Raman Spectrosc.*, 2014, **45**(1), 22–31, DOI: **10.1002/jrs.4423**.

27 T. Mino, Y. Saito and P. Verma, Quantitative analysis of polarization-controlled tip-enhanced Raman imaging through the evaluation of the tip dipole, *ACS Nano*, 2014, **8**(10), 10187–10195, DOI: **10.1021/nn5031803**.

28 Z. Lu, J. Ji, H. Ye, H. Zhang, S. Zhang and H. Xu, Quantifying the ultimate limit of plasmonic near-field enhancement, *Nat. Commun.*, 2024, **15**(1), 8803, DOI: **10.1038/s41467-024-53210-8**.

29 D. Roy, J. Wang and C. Williams, Novel methodology for estimating the enhancement factor for tip-enhanced Raman spectroscopy, *J. Appl. Phys.*, 2009, **105**(1), 013530, DOI: **10.1063/1.3056155**.

30 Y. Yokota, N. Hayazawa, B. Yang, E. Kazuma, F. C. I. Catalan and Y. Kim, Systematic assessment of benzenethiol self-assembled monolayers on Au(111) as a standard sample for electrochemical tip-enhanced Raman spectroscopy, *J. Phys. Chem. C*, 2019, **123**(5), 2953–2963, DOI: **10.1021/acs.jpcc.8b10829**.

31 H. Miranda, C. Rabelo, L. G. Cançado, T. L. Vasconcelos, B. S. Oliveira, F. Schulz, H. Lange, S. Reich, P. Kusch and A. Jorio, Impact of substrate on tip-enhanced Raman spectroscopy: A comparison between field-distribution simulations and graphene measurements, *Phys. Rev. Res.*, 2020, **2**(2), 023408, DOI: **10.1103/PhysRevResearch.2.023408**.

32 K. F. Mak, C. Lee, J. Hone, J. Shan and T. F. Heinz, Atomically thin MoS_2: a new direct-gap semiconductor, *Phys. Rev. Lett.*, 2010, **105**(13), 136805, DOI: 10.1103/PhysRevLett.105.136805.

33 E. del Corro, H. Terrones, A. Elias, C. Fantini, S. Feng, M. A. Nguyen, T. E. Mallouk, M. Terrones and M. A. Pimenta, Excited excitonic states in 1L, 2L, 3L, and bulk WSe_2 observed by resonant Raman spectroscopy, *ACS Nano*, 2014, **8**(9), 9629–9635, DOI: 10.1021/nn504088g.

34 H. Terrones, E. D. Corro, S. Feng, J. M. Poumirol, D. Rhodes, D. Smirnov, N. R. Pradhan, Z. Lin, M. A. T. Nguyen, A. L. Elías, *et al.*, New first order Raman-active modes in few layered transition metal dichalcogenides, *Sci. Rep.*, 2014, **4**(1), 4215, DOI: 10.1038/srep04215.

35 X. Zhang, X.-F. Qiao, W. Shi, J.-B. Wu, D.-S. Jiang and P.-H. Tan, Phonon and Raman scattering of two-dimensional transition metal dichalcogenides from monolayer, multilayer to bulk material, *Chem. Soc. Rev.*, 2015, **44**(9), 2757–2785, DOI: 10.1039/C4CS00282B.

36 A. Castellanos-Gomez, M. Buscema, R. Molenaar, V. Singh, L. Janssen, H. S. J. van der Zant and G. A. Steele, Deterministic transfer of two-dimensional materials by all-dry viscoelastic stamping, *2D Mater.*, 2014, **1**(1), 011002, DOI: 10.1088/2053-1583/1/1/011002.

37 E. del Corro, A. Botello-Méndez, Y. Gillet, A. L. Elias, H. Terrones, S. Feng, C. Fantini, D. Rhodes, N. Pradhan, L. Balicas, *et al.*, Atypical exciton–phonon interactions in WS_2 and WSe_2 monolayers revealed by resonance Raman spectroscopy, *Nano Lett.*, 2016, **16**(4), 2363–2368, DOI: 10.1021/acs.nanolett.5b05096.

38 L. P. McDonnell, J. J. S. Viner, P. Rivera, X. Xu and D. C. Smith, Observation of intravalley phonon scattering of 2s excitons in $MoSe_2$ and WSe_2 monolayers, *2D Mater.*, 2020, **7**(4), 045008, DOI: 10.1088/2053-1583/ab98f0.

39 M. De Luca, X. Cartoixà, J. Martín-Sánchez, M. López-Suárez, R. Trotta, R. Rurali and I. Zardo, New insights in the lattice dynamics of monolayers, bilayers, and trilayers of WSe_2 and unambiguous determination of few-layer-flakes' thickness, *2D Mater.*, 2020, **7**(2), 025004, DOI: 10.1088/2053-1583/ab5dec.

40 W. Zhao, Z. Ghorannevis, K. K. Amara, J. R. Pang, M. Toh, X. Zhang, C. Kloc, P. H. Tan and G. Eda, Lattice dynamics in mono- and few-layer sheets of WS_2 and WSe_2, *Nanoscale*, 2013, **5**(20), 9677–9683, DOI: 10.1039/C3NR03052K.

41 Z. Yang, J. Aizpurua and H. Xu, Electromagnetic field enhancement in TERS configurations, *J. Raman Spectrosc.*, 2009, **40**(10), 1343–1348, DOI: 10.1002/jrs.2429.

42 J. Yi, E.-M. You, R. Hu, D.-Y. Wu, G.-K. Liu, Z.-L. Yang, H. Zhang, Y. Gu, Y.-H. Wang, X. Wang, *et al.*, Surface-enhanced Raman spectroscopy: a half-century historical perspective, *Chem. Soc. Rev.*, 2025, **54**(3), 1453–1551, DOI: 10.1039/D4CS00883A.

43 R. Chen and L. Jensen, Interpreting chemical enhancements of surface-enhanced Raman scattering, *Chem. Phys. Rev.*, 2023, **4**(2), 021305, DOI: 10.1063/5.0138501.

44 J. Kerfoot, T. James, T. Taniguchi, K. Watanabe, P. H. Beton, G. A. Rance and M. W. George, Imaging the photophysics of organic semiconductors using polarisation-resolved and near-field optical spectroscopies, *Opt. Commun.*, 2025, **588**, 131945, DOI: 10.1016/j.optcom.2025.131945.

45 A. Jain, P. Bharadwaj, S. Heeg, M. Parzefall, T. Taniguchi, K. Watanabe and L. Novotny, Minimizing residues and strain in 2D materials transferred from PDMS, *Nanotechnology*, 2018, **29**(26), 265203, DOI: 10.1088/1361-6528/aabd90.

46 M. Rahaman, O. Selyshchev, Y. Pan, R. Schwartz, I. Milekhin, A. Sharma, G. Salvan, S. Gemming, T. Korn and D. R. T. Zahn, Observation of room-temperature dark exciton emission in nanopatch-decorated monolayer WSe_2 on metal substrate, *Adv. Opt. Mater.*, 2021, **9**(24), 2101801, DOI: 10.1002/adom.202101801.

47 Y. Huang, Y.-H. Pan, R. Yang, L.-H. Bao, L. Meng, H.-L. Luo, Y.-Q. Cai, G.-D. Liu, W.-J. Zhao, Z. Zhou, *et al.*, Universal mechanical exfoliation of large-area 2D crystals, *Nat. Commun.*, 2020, **11**(1), 2453, DOI: 10.1038/s41467-020-16266-w.

48 M. Velický, G. E. Donnelly, W. R. Hendren, S. McFarland, D. Scullion, W. J. I. DeBenedetti, G. C. Correa, Y. Han, A. J. Wain, M. A. Hines, *et al.*, Mechanism of gold-assisted exfoliation of centimeter-sized transition-metal dichalcogenide monolayers, *ACS Nano*, 2018, **12**(10), 10463–10472, DOI: 10.1021/acsnano.8b06101.

49 A. Rodriguez, M. Velický, J. Řáhová, V. Zólyomi, J. Koltai, M. Kalbáč and O. Frank, Activation of Raman modes in monolayer transition metal dichalcogenides through strong interaction with gold, *Phys. Rev. B*, 2022, **105**(19), 195413, DOI: 10.1103/PhysRevB.105.195413.

50 A. G. Milekhin, M. Rahaman, E. E. Rodyakina, A. V. Latyshev, V. M. Dzhagan and D. R. T. Zahn, Giant gap-plasmon tip-enhanced Raman scattering of MoS_2 monolayers on Au nanocluster arrays, *Nanoscale*, 2018, **10**(6), 2755–2763, DOI: 10.1039/C7NR06640F.

51 K.-D. Park, M. A. May, H. Leng, J. Wang, J. A. Kropp, T. Gougousi, M. Pelton and M. B. Raschke, Tip-enhanced strong coupling spectroscopy, imaging, and control of a single quantum emitter, *Sci. Adv.*, 2019, **5**(7), eaav5931, DOI: 10.1126/sciadv.aav5931.

52 L. Meng and M. Sun, Tip-enhanced photoluminescence spectroscopy of monolayer MoS_2, *Photon. Res.*, 2017, **5**(6), 745–749, DOI: 10.1364/PRJ.5.000745.

53 A. M. Dadgar, D. Scullion, K. Kang, D. Esposito, E. H. Yang, I. P. Herman, M. A. Pimenta, E. J. G. Santos and A. N. Pasupathy, Strain engineering and Raman spectroscopy of monolayer transition metal dichalcogenides, *Chem. Mater.*, 2018, **30**(15), 5148–5155, DOI: 10.1021/acs.chemmater.8b01672.

54 B. Aslan, C. Yule, Y. Yu, Y. J. Lee, T. F. Heinz, L. Cao and M. L. Brongersma, Excitons in strained and suspended monolayer WSe_2, *2D Mater.*, 2022, **9**(1), 015002, DOI: 10.1088/2053-1583/ac2d15.

55 Y. Pan, M. Rahaman, L. He, I. Milekhin, G. Manoharan, M. A. Aslam, T. Blaudeck, A. Willert, A. Matković, T. I. Madeira, *et al.*, Exciton tuning in monolayer WSe_2 via substrate induced electron doping, *Nanoscale Adv.*, 2022, **4**(23), 5102–5108, DOI: 10.1039/D2NA00495J.

56 F. J. R. Costa, T. G. L. Brito, I. D. Barcelos and L. F. Zagonel, Impacts of dielectric screening on the luminescence of monolayer WSe_2, *Nanotechnology*, 2023, **34**(38), 385703, DOI: 10.1088/1361-6528/acda3b.

57 X.-X. Zhang, T. Cao, Z. Lu, Y.-C. Lin, F. Zhang, Y. Wang, Z. Li, J. C. Hone, J. A. Robinson, D. Smirnov, *et al.*, Magnetic brightening and control of dark excitons in monolayer WSe_2, *Nat. Nanotechnol.*, 2017, **12**(9), 883–888, DOI: 10.1038/nnano.2017.105.

58 M. Barbone, A. R. P. Montblanch, D. M. Kara, C. Palacios-Berraquero, A. R. Cadore, D. De Fazio, B. Pingault, E. Mostaani, H. Li, B. Chen, *et al.*, Charge-tuneable biexciton complexes in monolayer WSe_2, *Nat. Commun.*, 2018, **9**(1), 3721, DOI: 10.1038/s41467-018-05632-4.

59 M. Rahaman, R. D. Rodriguez, G. Plechinger, S. Moras, C. Schüller, T. Korn and D. R. T. Zahn, Highly localized strain in a MoS_2/Au heterostructure revealed by tip-enhanced Raman spectroscopy, *Nano Lett.*, 2017, **17**(10), 6027–6033, DOI: 10.1021/acs.nanolett.7b02322.

60 K.-D. Park, T. Jiang, G. Clark, X. Xu and M. B. Raschke, Radiative control of dark excitons at room temperature by nano-optical antenna-tip Purcell effect, *Nat. Nanotechnol.*, 2018, **13**(1), 59–64, DOI: 10.1038/s41565-017-0003-0.

61 T. P. Darlington, C. Carmesin, M. Florian, E. Yanev, O. Ajayi, J. Ardelean, D. A. Rhodes, A. Ghiotto, A. Krayev, K. Watanabe, *et al.*, Imaging strain-localized excitons in nanoscale bubbles of monolayer WSe_2 at room temperature, *Nat. Nanotechnol.*, 2020, **15**(10), 854–860, DOI: 10.1038/s41565-020-0730-5.

62 W. Su, N. Kumar, S. Mignuzzi, J. Crain and D. Roy, Nanoscale mapping of excitonic processes in single-layer MoS_2 using tip-enhanced photoluminescence microscopy, *Nanoscale*, 2016, **8**(20), 10564–10569, DOI: 10.1039/C5NR07378B.

63 M. Velický, A. Rodriguez, M. Bouša, A. V. Krayev, M. Vondráček, J. Honolka, M. Ahmadi, G. E. Donnelly, F. Huang, H. D. Abruña, *et al.*, Strain and charge doping fingerprints of the strong interaction between monolayer MoS_2 and gold, *J. Phys. Chem. Lett.*, 2020, **11**(15), 6112–6118, DOI: 10.1021/acs.jpclett.0c01287.

64 S. Wood, F. Richheimer, T. Vincent, V. Tong, A. Catanzaro, Y. Cao, O. Kazakova and F. Araujo de Castro, Curvature-enhanced localised emission from dark states in wrinkled monolayer WSe_2 at room temperature, *Sci. Technol. Adv. Mater.*, 2023, **24**(1), 2278443, DOI: 10.1080/14686996.2023.2278443.

65 K.-D. Park, O. Khatib, V. Kravtsov, G. Clark, X. Xu and M. B. Raschke, Hybrid tip-enhanced nanospectroscopy and nanoimaging of monolayer WSe_2 with local strain control, *Nano Lett.*, 2016, **16**(4), 2621–2627, DOI: 10.1021/acs.nanolett.6b00238.

66 K. Hasz, Z. Hu, K.-D. Park and M. B. Raschke, Tip-enhanced dark exciton nanoimaging and local strain control in monolayer WSe_2, *Nano Lett.*, 2023, **23**(1), 198–204, DOI: 10.1021/acs.nanolett.2c03959.

67 W. Zhang, X. Cui, B.-S. Yeo, T. Schmid, C. Hafner and R. Zenobi, Nanoscale roughness on metal surfaces can increase tip-enhanced Raman scattering by an order of magnitude, *Nano Lett.*, 2007, **7**(5), 1401–1405, DOI: 10.1021/nl070616n.

68 I. Irfan, S. Golovynskyi, O. A. Yeshchenko, M. Bosi, T. Zhou, B. Xue, B. Li, J. Qu and L. Seravalli, Plasmonic enhancement of exciton and trion photoluminescence in 2D MoS_2 decorated with Au nanorods: impact of nonspherical shape, *Phys. E*, 2022, **140**, 115213, DOI: 10.1016/j.physe.2022.115213.

69 Z. Wang, Y. Liu, D. Chen, Z. Wang, M. Asbahi, S. D. Rezaei, J. Deng, J. Teng, A. T. S. Wee, W. Zhang, *et al.*, Nanocavity-induced trion emission from atomically thin WSe_2, *Sci. Rep.*, 2022, **12**(1), 15861, DOI: 10.1038/s41598-022-20226-3.

70 J. Shi, J. Zhu, X. Wu, B. Zheng, J. Chen, X. Sui, S. Zhang, J. Shi, W. Du, Y. Zhong, *et al.*, Enhanced trion emission and carrier dynamics in monolayer WS_2 coupled with plasmonic nanocavity, *Adv. Opt. Mater.*, 2020, **8**(23), 2001147, DOI: 10.1002/adom.202001147.

71 T. W. Lo, X. Chen, Z. Zhang, Q. Zhang, C. W. Leung, A. V. Zayats and D. Lei, Plasmonic nanocavity induced coupling and boost of dark excitons in monolayer WSe_2 at room temperature, *Nano Lett.*, 2022, **22**(5), 1915–1921, DOI: 10.1021/acs.nanolett.1c04360.

72 J. Zhou, J. C. Thomas, E. Barre, E. S. Barnard, A. Raja, S. Cabrini, K. Munechika, A. Schwartzberg and A. Weber-Bargioni, Near-field coupling with a nanoimprinted probe for dark exciton nanoimaging in monolayer WSe_2, *Nano Lett.*, 2023, **23**(11), 4901–4907, DOI: 10.1021/acs.nanolett.3c00621.

73 A. W. Dweydari and C. H. B. Mee, Work function measurements on (100) and (110) surfaces of silver, *Phys. Status Solidi A*, 1975, **27**(1), 223–230, DOI: 10.1002/pssa.2210270126.

74 H. B. Michaelson, The work function of the elements and its periodicity, *J. Appl. Phys.*, 1977, **48**(11), 4729–4733, DOI: 10.1063/1.323539.